

Broken Symmetry in Ideal Chern Bands

Hui Liu,¹ Kang Yang,² Ahmed Abouelkomsan,³ Zhao Liu,^{4,*} and Emil J. Bergholtz^{1,†}

¹Department of Physics, Stockholm University, AlbaNova University Center, 106 91 Stockholm, Sweden

²Dahlem Center for Complex Quantum Systems and Fachbereich Physik, Freie Universität Berlin, 14195 Berlin, Germany

³Department of Physics, Massachusetts Institute of Technology, Cambridge, Massachusetts 02139, USA

⁴Zhejiang Institute of Modern Physics, Zhejiang University, Hangzhou 310058, China

(Dated: February 27, 2024)

Recent observations of the fractional anomalous quantum Hall effect in moiré materials have reignited the interest in fractional Chern insulators (FCIs). The chiral limit in which analytic Landau level-like single-particle states form an “ideal” Chern band and local interactions lead to Laughlin-like FCIs at $1/3$ filling, has been very useful for understanding these systems by relating them to the lowest Landau level. We show, however, that, even in the idealized chiral limit, a fluctuating quantum geometry is associated with strongly broken symmetries and a phenomenology very different from that of Landau levels. In particular, particle-hole symmetry is strongly violated and e.g. at $2/3$ filling an emergent interaction driven Fermi liquid state with no Landau level counterpart is energetically favoured. In fact, even the exact Laughlin-like zero modes at $1/3$ filling have a non-uniform density tracking the underlying quantum geometry. Moreover, by switching to a Coulomb interaction, the ideal Chern band features charge density wave states with no lowest Landau level counterpart.

Introduction. — The rapid development of techniques to fabricate van-der-Waals heterostructures with moiré patterns is providing excitingly new opportunities to realize and manipulate novel quantum phases of matter [1, 2]. Fractional Chern insulators (FCIs) [3–13], which are lattice analogues of the celebrated fractional quantum Hall (FQH) states in continuum two-dimensional electron gases (2DEGs) [14–16], have been theoretically predicted and experimentally observed in graphene [17–22] and transition metal dichalcogenide moiré materials [23–28]. The exciting experimental evidence of FCIs has further attracted tremendous theoretical attention to understand the phenomena emerging in experiments [29–37].

Based on the analogy between FCIs and the FQH states, the emergence of FCI states in moiré materials suggests the similarity of the partially filled moiré band to a Landau level (LL) in 2DEGs [19, 38, 39]. This similarity imposes strong conditions on the dispersion, topology, and quantum geometry [19, 38, 40–54] of the moiré band. In general, a moiré band is expected to mimic a LL if (i) it is nearly flat in dispersion; (ii) it carries a nonzero Chern number; (iii) its quantum geometry, characterized by the Berry curvature and the Fubini-Study (FS) metric [55, 56], is nearly uniform in the entire Brillouin zone (BZ); and (iv) its FS metric varies approximately in sync with the Berry curvature. The last two conditions originate from the special quantum geometry of a LL, i.e., the Berry curvature Ω and the FS metric g are constant and related to each other by $g_{ij} = (n + \frac{1}{2}) |\Omega| \delta_{ij}$, where n is the LL index [44].

According to the criteria above, twisted bilayer graphene in the chiral limit (cTBG) [57] stands out as an extremely promising platform to realize the LL physics in moiré systems. The valence and conduction bands of cTBG are perfectly flat at magic twist angles [57] and carry unit Chern numbers. Furthermore, their quantum geometry are “ideal” [19, 38] in the sense that the FS metric varies exactly in sync with the Berry curvature at each \mathbf{k} point of the BZ via $g_{ij}(\mathbf{k}) = \frac{1}{2} |\Omega(\mathbf{k})| \delta_{ij}$, although $g(\mathbf{k})$ and $\Omega(\mathbf{k})$ still fluctu-

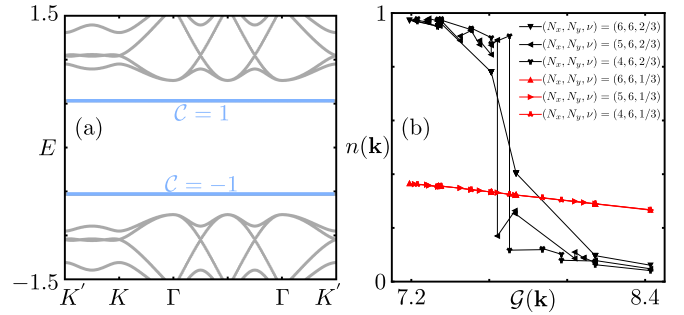


FIG. 1. Broken symmetry in an ideal Chern band. (a) Moiré band structure of cTBG at the first magic angle $\theta \approx 1.13^\circ$ and $m_z = 0.1$ eV. The horizontal lines are the two flat bands with Chern number $C = \pm 1$. (b) Our main result: the occupation number of the many-body ground state $n(\mathbf{k})$ as a function of the quantum geometry, $G(\mathbf{k}) \equiv \log[\text{tr}[g(\mathbf{k})]] = \log[|\Omega(\mathbf{k})|]$, for a FCI state at filling $\nu = 1/3$ of the $C = -1$ band and an emergent Fermi liquid at $\nu = 2/3$. This shows that ideal Chern bands strongly breaks both the reciprocal-space translation symmetry and the particle-hole symmetry that are present in Landau levels.

ate with \mathbf{k} [19]. The cTBG bands are hence almost identical to the $n = 0$ lowest LL (LLL) except that their quantum geometry is not uniform. These elegant properties lead to LLL-like single-body wave functions, and exact zero modes for pseudopotential-like short-range interactions in cTBG flat bands, just like the Laughlin states in the LLL [38]. The ideal quantum geometry also emerges for flat bands with higher Chern number in the chiral limit of multilayered graphene [48, 49]. While the aforementioned effective continuum descriptions are most relevant for moiré systems, the Kapit-Mueller model [10] and arbitrary Chern number generalizations thereof [58] provide analogous ideal band geometry in tight-binding models and exact parent Hamiltonians for bosonic states. In general, ideal Chern bands have been described as LLLs in curved space [52].

Given the glaring similarity between the ideal flat bands in

cTBG [cf. Fig. 1(a)] and the LLL, one may naturally expect that their only difference, namely, the fluctuating quantum geometry of the former, would not cause significantly distinct physics in cTBG flat bands from that in the LLL. However, in this work we present strong evidence against this expectation. We find that the particle-hole symmetry in a single cTBG flat band is still strikingly broken by the non-uniform, albeit ideal quantum geometry [see Fig. 1(b)]. Remarkably, even a pseudopotential-like local interaction can induce an unconventional Fermi liquid state at band filling $\nu = 2/3$ with no LL counterpart [59]. The ground state at $\nu = 1/3$ remains an exact zero-energy Laughlin-like state — which, however, also exhibits a non-uniform particle density caused by the fluctuating FS metric tensor [Fig. 1(b)]. Furthermore, the Coulomb interaction favors a charge density wave instead of the composite Fermi liquid at $\nu = 1/4$, which again distinguishes the cTBG ideal bands from the LLL.

Setup. — The valley and spin polarized Hamiltonian of cTBG takes the form of [57]

$$H = \begin{pmatrix} -v_F \sigma_{\theta/2} \cdot \nabla & wT(\mathbf{r}) \\ wT^\dagger(\mathbf{r}) & -iv_F \sigma_{-\theta/2} \cdot \nabla \end{pmatrix}, \quad (1)$$

where $\sigma_{\theta/2} = e^{-i\theta\sigma_z/4}(\sigma_x, \sigma_y)e^{i\theta\sigma_z/4}$ and v_F is the Fermi velocity of monolayer graphene. $T(\mathbf{r}) = \sum_{n=1}^3 T_n e^{-i\mathbf{q}_n \cdot \mathbf{r}}$ describes the coupling between the two layers, where $T_{n+1} = \kappa\sigma_0 + \cos(n\phi)\sigma_x + \sin(n\phi)\sigma_y$ with $\phi = 2\pi/3$, $\mathbf{q}_1 = k_\theta(0, -1)$, and $\mathbf{q}_{2,3} = k_\theta(\pm\sqrt{3}/2, 1/2)$. We fix $w = 0.11$ eV. The size of moiré Brillouin zone (MBZ) is controlled by $k_\theta = 2k_D \sin(\theta/2)$, where $k_D = 4\pi/(3a_0)$ with a_0 the graphene lattice constant. The lattice constant of the moiré pattern is $a_M = a_0/(2 \sin(\theta/2))$.

We focus on the chiral limit by setting $\kappa = 0$ and work at the first magic angle [57] throughout the paper. In this case, the valence and conduction bands are perfectly flat with zero energy and possess ideal quantum geometry. Introducing an extra sublattice potential $m_z \tau_0 \sigma_z$, where τ_0 acting on the layer index, can lift the two-fold degeneracy, leading to two isolated flat bands with Chern number -1 and $+1$, respectively [see Fig. 1(a)]. The precise value of m_z does not affect our results because it only shifts the band energy by a constant without changing the band eigenvector.

Without losing generality, we consider the interacting physics in the lower flat band. We project the electron-electron interaction to this single valence band and reach

$$H^{\text{proj}} = \sum_{\mathbf{k}} V_{\mathbf{k}_1 \mathbf{k}_2 \mathbf{k}_3 \mathbf{k}_4} c_{\mathbf{k}_1}^\dagger c_{\mathbf{k}_2}^\dagger c_{\mathbf{k}_3} c_{\mathbf{k}_4}, \quad (2)$$

with $c_{\mathbf{k}}^\dagger$ ($c_{\mathbf{k}}$) being the fermionic creation (annihilation) operator with momentum \mathbf{k} in the valence band. The normal ordering convention here is consistent with obtaining exact zero-modes at $\nu = 1/3$ [19]. The band eigenvectors have been encoded into the matrix element $V_{\mathbf{k}_1 \mathbf{k}_2 \mathbf{k}_3 \mathbf{k}_4}$ (see the Supplemental Material [60] for more details). The single-electron dispersion is dropped because it only contributes a constant. We use exact diagonalization to extract the low-lying energy spectrum

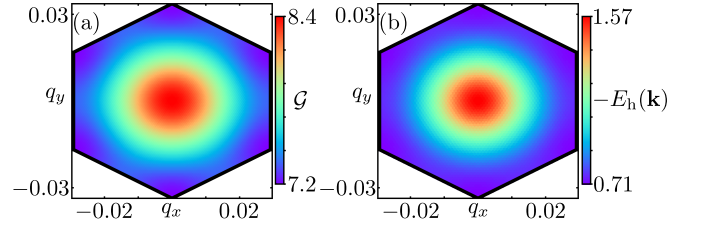


FIG. 2. **Quantum geometry and single hole dispersion.** (a) The quantum geometry $\mathcal{G}(\mathbf{k})$ and (b) the single hole energy $-E_h(\mathbf{k})$ as a function of momentum $\mathbf{k} = (q_x, q_y)$.

and the associated eigenstates for finite systems including N electrons in N_s moiré unit cells at band filling $\nu = N/N_s$, which can provide direct evidence to distinguish FCIs from competing phases, such as the Fermi liquid and the charge density wave, etc.

Broken symmetry in ideal Chern bands. — Our main result centers around the striking breaking of reciprocal-space translation symmetry and particle-hole symmetry in the ideal flat band of cTBG, even when we employ a pseudopotential-like short-range repulsive interaction whose Fourier transform is $V(\mathbf{q}) = V_0 - V_1 a_M^2 |\mathbf{q}|^2$ [19, 60, 61]. While this interaction gives rise to zero-energy Laughlin-like model FCIs at band filling $\nu = 1/3$, the particle occupation number $n(\mathbf{k})$ is not a constant at $1/3$ as for the conventional Laughlin state in the LLL. By contrast, $n(\mathbf{k})$ exhibits a clear linear dependence on the quantum geometry characterized by $\mathcal{G}(\mathbf{k}) \equiv \log[\text{tr}[g(\mathbf{k})]] = \log[|\Omega(\mathbf{k})|]$ [Fig. 1(b)]. This variation of $n(\mathbf{k})$ is a signature of the breaking of translation symmetry in the reciprocal space, which further suggests a significant center-of-mass dependence of the model Laughlin-like wavefunction within the ideal flat of cTBG [19, 38]. Notably, as shown in Fig. 2 the quantum geometry in terms of \mathcal{G} [Fig. 2(a)], has a similar structure in the moiré BZ as the energy of a single hole [Fig. 2(b)], thus providing a physical rationale for the inhomogeneous (reciprocal space) occupation density $n(\mathbf{k})$ [51].

Moving to banding filling $\nu = 2/3$, we find that the occupation number $n(\mathbf{k})$ completely deviates from the value $2/3$ of the $\nu = 2/3$ FQH state in the LLL. Instead, as displayed in Fig. 1(b), a sharp jump from $n(\mathbf{k}) \approx 1$ to $n(\mathbf{k}) \approx 0$ signifies the emergence of a Fermi liquid, with a stable Fermi surface around $\mathcal{G} \approx 7.6$. The very distinct behavior of $n(\mathbf{k})$ at $\nu = 2/3$ from that at $\nu = 1/3$ indicates the breaking of particle-hole symmetry in the ideal cTBG bands. Such particle-hole asymmetry in Chern bands has been identified in various non-ideal models: first in a checkerboard lattice [59] and, recently, in moiré systems [17, 62] where it is related to the fluctuating quantum geometry [51]. That these effects persist even for electrons with pseudopotential-like interaction in the ideal cTBG bands further emphasizes the fundamental difference between Chern bands and the LLL, and disapproves of the overoptimistic expectation that the LLL physics can be perfectly reproduced in the cTBG band given the ideal quan-

tum geometry and the Laughlin-like wave functions in the latter.

Evidence for the FCIs and the emergent Fermi liquid. — We now provide more numerical evidence on the FCIs at $\nu = 1/3$ and the Fermi liquid at $\nu = 2/3$ in the cTBG ideal band. The interaction is still chosen as the pseudopotential-like local repulsion $V(\mathbf{q}) = V_0 - V_1 a_M^2 |\mathbf{q}|^2$.

The most straightforward signature of the $\nu = 1/3$ Laughlin-like model FCIs is the three exactly zero-energy ground states with momenta predicted by the Haldane statistics [8, 63]. This can be clearly seen in the low-lying energy spectrum for any finite system [Fig. 3(a)]. The ground-state topological order can be further diagnosed by the particle-cut entanglement spectrum [64, 65]. Here, we divide the whole system into N_A and $N_B = N - N_A$ electrons. By tracing out the subsystem B , we effectively create holes in the system, so the reduced density matrix of the subsystem A , $\rho_A = \text{tr}_B[\frac{1}{3} \sum_{i=1}^3 |\Psi_i\rangle\langle\Psi_i|]$, contains the information of the quasihole excitations above the ground states $|\Psi_i\rangle$. In Fig. 3(b), we display the particle-cut entanglement spectrum, which is the spectrum of $-\log \rho_A$, for the three zero modes. There is a narrow band at the bottom of the entanglement spectrum, in which the number of levels matches the quasihole counting of the $\nu = 1/3$ Laughlin state. More entanglement levels appear at very high entanglement energies above $\xi \approx 50$. However, as these levels correspond to exponentially small eigenvalues of ρ_A beyond the machine precision limit, we attribute them to numerical noise. Therefore, the entanglement spectrum of the zero modes at $\nu = 1/3$ in fact has an infinite entanglement gap, which is a remarkable feature of model wavefunctions [58, 64]. Both the energy spectrum and the ground-state entanglement spectrum strongly indicate the existence of Laughlin-like model FCIs at $\nu = 1/3$ and rule out the possibility of a trivial charge density wave.

At band filling $\nu = 2/3$, the absence of topological degeneracy in the energy spectrum, as illustrated in Fig. 3(c), already rules out the presence of FCIs. Given the dispersionless nature of the ideal cTBG band, the Fermi liquid feature in Fig. 1(b) must originate solely from the electron-electron correlation, whose role can be exposed more clearly in the hole picture. It has been pointed out in early works that the electron-electron interaction leads to an extra single-hole dispersion $E_h(\mathbf{k}) = \sum_{\mathbf{k}' \in \text{MBZ}} (V_{\mathbf{k}'\mathbf{k}\mathbf{k}'} + V_{\mathbf{k}\mathbf{k}'\mathbf{k}} - V_{\mathbf{k}\mathbf{k}'\mathbf{k}'} - V_{\mathbf{k}'\mathbf{k}\mathbf{k}})$ after the particle-hole transformation [17, 59]. This hole dispersion in general dominates over the hole-hole interaction at relatively large fillings and gives rise to the correlation-induced Fermi liquid. We confirm the correlated nature of the Fermi liquid in cTBG ideal bands by drawing the ground-state occupation number of electrons as a function of $E_h(\mathbf{k})$. As shown in Fig. 3(d), $n(\mathbf{k})$ at $\nu = 2/3$ has an overall trend to drop from 1 to 0 following the hole dispersion $E_h(\mathbf{k})$. The zigzags in $n(\mathbf{k})$ for some system sizes result from the hole-hole interaction which distorts the Fermi surface of electrons. In contrast, $n(\mathbf{k})$ for the $\nu = 1/3$ FCI only weakly varies with the hole dispersion. The Fermi liquid behavior at $\nu = 2/3$ even extends beyond the ground state, where ex-

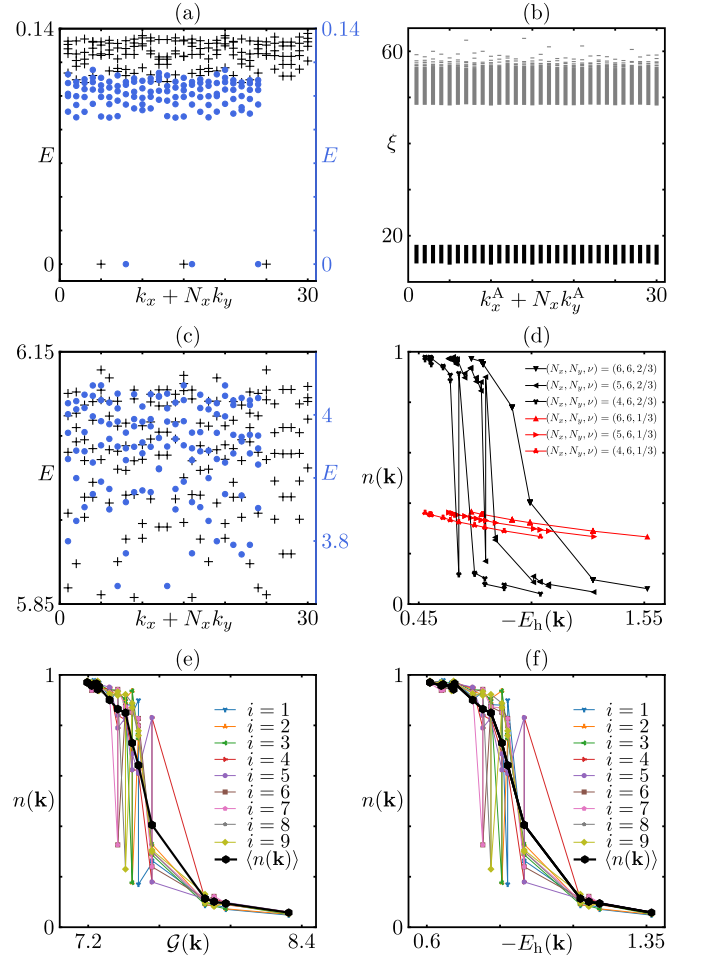


FIG. 3. FCIs and Fermi Liquids. (a) The many-body energy spectrum at band filling $\nu = 1/3$ on the 4×6 (blue \cdot) and 5×6 clusters (black $+$), respectively. We calculate five lowest energies in each momentum sector. (b) The associated particle-cut entanglement spectrum of the three zero modes on the 5×6 cluster for $N_A = 5$. The number of levels in the narrow band at the bottom is 23256, which matches the quasihole counting of the $\nu = 1/3$ Laughlin state. The very high-energy grey levels are numerical noises. (c) The many-body energy spectrum at band filling $\nu = 2/3$. (d) The ground-state occupation number of electrons at $\nu = 1/3$ and $\nu = 2/3$ as a function of single-hole energy. (e-f) The occupation number of electrons for the lowest 9 excited states at $\nu = 2/3$ on the 5×6 cluster as a function of the quantum geometry and the single-hole energy, respectively. Here, the black hexagon and the bold line represent the averaged occupation number over the lowest 20 energy states.

cited states possess features of particle-hole excitations near the emergent Fermi surface [see Figs. 3(e) and (f)].

We emphasize that the symmetry breaking in cTBG ideal bands with pseudopotential-like interactions is a phenomenon observed across various fillings. For the filling $\nu \in [1/3, 1/2]$, such as $\nu = 2/5$ and $3/7$, and their complements, our results show a consistent behavior, where an FCI emerges at band filling ν but disappears at band filling $1 - \nu$ (see the SM for more details [60]).

Charge density wave at $\nu = 1/4$. — In previous sections,

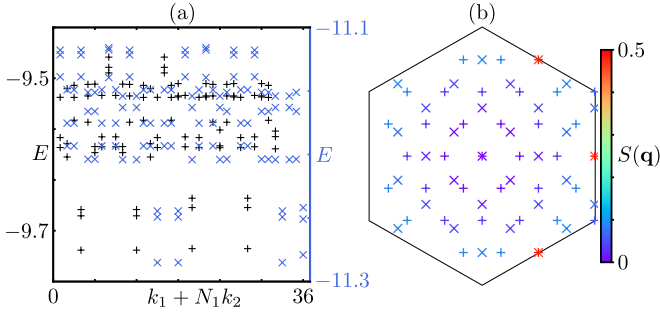


FIG. 4. **CDWs from the Coulomb interaction in the ideal cTBG band.** (a) The many-body energy spectrum at band filling $\nu = 1/4$ for the bare Coulomb interaction. We calculate three lowest levels in each momentum sector. (b) The ground-state structure factor in the MBZ. Here, we use tilted samples to include the three inequivalent \mathbf{M} points. The + (black in (a)) and \times (blue in (a)) symbols correspond to clusters with 32 and 36 moiré unit cells, respectively [60].

the striking differences between the ideal cTBG band and the LLL have been revealed at fillings where FQH states are expected in the LLL. Now we consider other fillings where there are no incompressible FQH states in the LLL. As a concrete example, we consider $\nu = 1/4$, where the Coulomb interaction $V_C(\mathbf{q}) \sim 1/|\mathbf{q}|$ in the LLL were found to stabilize the Fermi sea of composite fermions [66, 67] (except in the wide quantum well which is beyond the scope of our work). We suppose the electrons in the cTBG interact via the bare Coulomb potential also. Surprisingly, at $\nu = 1/4$ of the ideal cTBG band, we observe a charge density wave (CDW) rather than the Fermi sea of composite fermions.

We verify the CDW phase from two aspects. For finite samples whose single-electron momenta allowed by the periodic boundary conditions include the three inequivalent \mathbf{M} points of the MBZ, we find four approximately degenerate ground states in the low-energy spectrum separated by the momenta $\mathbf{M}_{i=1,2,3}$ [Fig. 4(a)]. This is a strong signal of the charge distribution with order momenta \mathbf{M}_i . The charge order can be diagnosed more reliably by the structure factor

$$S(\mathbf{q}) = \frac{1}{N_s} (\langle \rho(\mathbf{q}) \rho(-\mathbf{q}) \rangle - N^2 \delta_{\mathbf{q},0}), \quad (3)$$

where $\rho_{\mathbf{q}}$ is the density operator projected to the ideal cTBG band. Remarkably, we find pronounced peaks only at the three \mathbf{M} points [Fig. 4(b)], confirming the ground states as \mathbf{M} -CDWs. The unit cell of the charge distribution in these CDWs is quadrupled moiré unit cell. Similar CDWs were reported in realistic TBG beyond the chiral limit [68]. Our results demonstrate that they can survive even in the ideal cTBG band. The fluctuation of the Berry curvature and the quantum metric tensor of the ideal cTBG band, which distinguishes it from the LLL, could be a major mechanism for the formation of these CDWs that are absent in the LLL.

Discussion. — By employing both a pseudopotential-like short-range interaction and a Coulomb interaction, we have discovered that, even the topological flat band in cTBG ex-

hibits an ideal quantum geometry, yet significant dissimilarities persist when compared to the LLL. In the former scenario, the breaking of particle-hole symmetry at band filling $\nu = 2/3$ leads to a correlation-induced Fermi liquid, while at $\nu = 1/3$ a FCI is supported although also this state has a non-uniform occupation density adapting to the underlying geometry. The breakdown of correspondence between the flat band in cTBG and the LLL also provides hints to other possible competing orders in this ideal setting. In particular, we unveiled a charge density wave at band filling $\nu = 1/4$ in the latter case, characterized by three clear peaks in the structure factor. This contrasts with the anticipated gapless composite Fermi liquid of the LLL physics, highlighting compelling deviations in cTBG. In conclusion, while the ideal cTBG band does indeed elegantly preserve the presence of zero modes of certain short range interactions, the phase diagram is qualitatively altered compared to that of the LLL.

It should be noted that the quantum geometric quantities are of limited fundamental importance in lattice models due to their dependence on the embedding of the orbitals into real space. A more orbital-independent approach should go back to continuum models obtained from first principle calculations. In moiré systems, the underlying (e.g., graphene) orbitals are highly localized compared to the moiré length scale. Thus the system has a natural continuum description that for practical purposes alleviates the fundamental ambiguity of lattice embeddings.

We also note that normal ordering prescription matters. We have used a convention used in the literature, normal ordering with respect to an empty vacuum, which leads to Laughlin-like zero modes of electrons at $\nu = 1/3$ [19]. If instead normal ordered with respect to charge neutrality, the interaction Hamiltonian differs by extra single-particle terms which can be thought as Hartree Fock corrections from the remote bands [69] but the particle-hole asymmetry within the single band still exists hence our results still hold with the difference that FCIs are no longer exact zero modes of the pseudopotential. We stress that the particle-hole asymmetry considered here is the one emerging within a given (ideal) band which is different from the question of symmetry of the model as a whole.

The glaring differences between ideal Chern bands and Landau levels identified in this work prompts a natural question that, what criteria can accurately determine to what extent an ideal moiré Chern band aligns with the physics of the Landau levels more generally. Understanding this question becomes crucial in realization of non-Abelian topological phases and their associated quantum computing applications in moiré systems, which has been experimentally demonstrated that FCIs can be realized without the need of high magnetic field and exhibit robustness at relatively high temperatures.

While FCIs have been experimentally observed in twisted bilayer graphene [21] at fillings $\nu = 4 - 1/3$ and $\nu = 4 - 2/3$ of the conduction band, we would like to stress that our emphasis here is different as we are studying the spin and valley polarized limit of chiral TBG. It is believed that the state

at $\nu = 4 - 1/3$ is spin and valley polarized [70] while the state at $\nu = 4 - 2/3$ (in the chiral limit) is spin-singlet [18]. Our results are concerned with particle-hole asymmetry in a band with a single flavor. In the presence of multi-component degrees of freedom, the single-hole dispersion takes a more complicated form than the form in [71] therefore the conclusions can differ. It is also possible that external magnetic fields could diminish the existing particle-hole asymmetry at zero magnetic field approaching a more LLL-like limit. We leave this to future study.

On the other hand, robust spin-valley polarization has been observed in moiré TMD systems [25–28] but FCIs were found only at hole doping $\nu_h = 2/3$ of the valence band while absent at the particle-hole dual filling $\nu_h = 1/3$ reflecting strong particle-hole asymmetry similar to our study. While chiral TBG is significantly different from moiré TMDs, we believe that our results provide general and relevant insights to this problem. We have shown that even in an idealized model, translation and particle-hole symmetries is strongly violated even in absence of band mixing, hence such symmetries should not be expected in any model derived starting from an underlying lattice structure.

Acknowledgements.— We acknowledge discussions with Jie Wang. H. Liu and E. J. Bergholtz were supported by the Swedish Research Council (VR, grant 2018-00313), the Wallenberg Academy Fellows program of the Knut and Alice Wallenberg Foundation (2018.0460) and the Göran Gustafsson Foundation for Research in Natural Sciences and Medicine. Z. Liu was supported by the National Natural Science Foundation of China (Grant No. 12350403). K. Yang is supported by the ANR-DFG project (TWISTGRAPH). A. Abouelkomsan is supported by the Knut and Alice Wallenberg Foundation (2022.0348).

* zhaol@zju.edu.cn

† emil.bergholtz@fysik.su.se

- [1] A. K. Geim and I. V. Grigorieva, “Van der Waals heterostructures,” *Nature* **499**, 419–425 (2013), 1307.6718.
- [2] K. S. Novoselov, A. Mishchenko, A. Carvalho, and A. H. Castro Neto, “2D materials and van der Waals heterostructures,” *Science* **353** (2016), 10.1126/science.aac9439.
- [3] A. Kol and N. Read, “Fractional quantum hall effect in a periodic potential,” *Phys. Rev. B* **48**, 8890–8898 (1993).
- [4] E. Tang, J.-W. Mei, and X.-G. Wen, “High-Temperature Fractional Quantum Hall States,” *Physical Review Letters* **106**, 236802 (2011).
- [5] K. Sun, Z. Gu, H. Katsura, and S. Das Sarma, “Nearly flatbands with nontrivial topology,” *Phys. Rev. Lett.* **106**, 236803 (2011).
- [6] T. Neupert, L. Santos, C. Chamon, and C. Mudry, “Fractional quantum hall states at zero magnetic field,” *Phys. Rev. Lett.* **106**, 236804 (2011).
- [7] D. Sheng, Z.-C. Gu, K. Sun, and L. Sheng, “Fractional quantum hall effect in the absence of landau levels,” *Nature communications* **2**, 1–5 (2011).
- [8] N. Regnault and B. A. Bernevig, “Fractional chern insulator,” *Phys. Rev. X* **1**, 021014 (2011).
- [9] G. Möller and N. R. Cooper, “Composite fermion theory for bosonic quantum hall states on lattices,” *Phys. Rev. Lett.* **103**, 105303 (2009).
- [10] E. Kapit and E. Mueller, “Exact parent hamiltonian for the quantum hall states in a lattice,” *Phys. Rev. Lett.* **105**, 215303 (2010).
- [11] E. J. Bergholtz and Z. Liu, “Topological flat band models and fractional chern insulators,” *International Journal of Modern Physics B* **27**, 1330017 (2013).
- [12] S. A. Parameswaran, R. Roy, and S. L. Sondhi, “Fractional quantum hall physics in topological flat bands,” *Comptes Rendus Physique* **14**, 816–839 (2013), topological insulators / Isolants topologiques.
- [13] Z. Liu and E. J. Bergholtz, “Recent developments in fractional chern insulators,” in *Encyclopedia of Condensed Matter Physics (Second Edition)*, edited by T. Chakraborty (Academic Press, Oxford, 2024) second edition ed., pp. 515–538.
- [14] D. C. Tsui, H. L. Stormer, and A. C. Gossard, “Two-dimensional magnetotransport in the extreme quantum limit,” *Phys. Rev. Lett.* **48**, 1559–1562 (1982).
- [15] R. B. Laughlin, “Anomalous quantum hall effect: An incompressible quantum fluid with fractionally charged excitations,” *Phys. Rev. Lett.* **50**, 1395–1398 (1983).
- [16] T. H. Hansson, M. Hermanns, S. H. Simon, and S. F. Viefers, “Quantum hall physics: Hierarchies and conformal field theory techniques,” *Rev. Mod. Phys.* **89**, 025005 (2017).
- [17] A. Abouelkomsan, Z. Liu, and E. J. Bergholtz, “Particle-hole duality, emergent fermi liquids, and fractional chern insulators in moiré flatbands,” *Phys. Rev. Lett.* **124**, 106803 (2020).
- [18] C. Repellin and T. Senthil, “Chern bands of twisted bilayer graphene: Fractional Chern insulators and spin phase transition,” *Physical Review Research* **2**, 023238 (2020).
- [19] P. J. Ledwith, G. Tarnopolsky, E. Khalaf, and A. Vishwanath, “Fractional chern insulator states in twisted bilayer graphene: An analytical approach,” *Phys. Rev. Research* **2**, 023237 (2020).
- [20] Z. Liu, A. Abouelkomsan, and E. J. Bergholtz, “Gate-tunable fractional chern insulators in twisted double bilayer graphene,” *Phys. Rev. Lett.* **126**, 026801 (2021).
- [21] Y. Xie, A. T. Pierce, J. M. Park, D. E. Parker, E. Khalaf, P. Ledwith, Y. Cao, S. H. Lee, S. Chen, P. R. Forrester, *et al.*, “Fractional chern insulators in magic-angle twisted bilayer graphene,” *Nature* **600**, 439–443 (2021).
- [22] Z. Lu, T. Han, Y. Yao, A. P. Reddy, J. Yang, J. Seo, K. Watanabe, T. Taniguchi, L. Fu, and L. Ju, “Fractional quantum anomalous hall effect in a graphene moire superlattice,” (2023), arXiv:2309.17436 [cond-mat.mes-hall].
- [23] H. Li, U. Kumar, K. Sun, and S.-Z. Lin, “Spontaneous fractional chern insulators in transition metal dichalcogenide moiré superlattices,” *Phys. Rev. Res.* **3**, L032070 (2021).
- [24] V. Crépel and L. Fu, “Anomalous hall metal and fractional chern insulator in twisted transition metal dichalcogenides,” *Phys. Rev. B* **107**, L201109 (2023).
- [25] J. Cai, E. Anderson, C. Wang, X. Zhang, X. Liu, W. Holtzmann, Y. Zhang, F. Fan, T. Taniguchi, K. Watanabe, Y. Ran, T. Cao, L. Fu, D. Xiao, W. Yao, and X. Xu, “Signatures of fractional quantum anomalous hall states in twisted mote2,” *Nature* **622**, 63–68 (2023).
- [26] Y. Zeng, Z. Xia, K. Kang, J. Zhu, P. Knüppel, C. Vaswani, K. Watanabe, T. Taniguchi, K. F. Mak, and J. Shan, “Thermodynamic evidence of fractional chern insulator in moirémote2,” *Nature* **622**, 69–73 (2023).
- [27] H. Park, J. Cai, E. Anderson, Y. Zhang, J. Zhu, X. Liu, C. Wang, W. Holtzmann, C. Hu, Z. Liu, T. Taniguchi, K. Watanabe, J.-H. Chu, T. Cao, L. Fu, W. Yao, C.-Z. Chang, D. Cobden, D. Xiao,

- and X. Xu, “Observation of fractionally quantized anomalous hall effect,” *Nature* **622**, 74–79 (2023).
- [28] F. Xu, Z. Sun, T. Jia, C. Liu, C. Xu, C. Li, Y. Gu, K. Watanabe, T. Taniguchi, B. Tong, J. Jia, Z. Shi, S. Jiang, Y. Zhang, X. Liu, and T. Li, “Observation of integer and fractional quantum anomalous hall effects in twisted bilayer mote_2 ,” *Phys. Rev. X* **13**, 031037 (2023).
- [29] Z. Dong, A. S. Patri, and T. Senthil, “Theory of fractional quantum anomalous hall phases in pentalayer rhombohedral graphene moiré structures,” (2023), [arXiv:2311.03445 \[cond-mat.str-el\]](#).
- [30] B. Zhou, H. Yang, and Y.-H. Zhang, “Fractional quantum anomalous hall effects in rhombohedral multilayer graphene in the moiréless limit and in coulomb imprinted superlattice,” (2023), [arXiv:2311.04217 \[cond-mat.str-el\]](#).
- [31] C. Wang, X.-W. Zhang, X. Liu, Y. He, X. Xu, Y. Ran, T. Cao, and D. Xiao, “Fractional chern insulator in twisted bilayer mote_2 ,” *Phys. Rev. Lett.* **132**, 036501 (2024).
- [32] A. P. Reddy, F. Alsallom, Y. Zhang, T. Devakul, and L. Fu, “Fractional quantum anomalous hall states in twisted bilayer mote_2 and wse_2 ,” *Phys. Rev. B* **108**, 085117 (2023).
- [33] N. Morales-Durán, J. Wang, G. R. Schleder, M. Angeli, Z. Zhu, E. Kaxiras, C. Repellin, and J. Cano, “Pressure-enhanced fractional chern insulators along a magic line in moiré transition metal dichalcogenides,” *Phys. Rev. Res.* **5**, L032022 (2023).
- [34] J. Yu, J. Herzog-Arbeitman, M. Wang, O. Vafek, B. A. Bernevig, and N. Regnault, “Fractional chern insulators vs. non-magnetic states in twisted bilayer mote_2 ,” (2023), [arXiv:2309.14429 \[cond-mat.mes-hall\]](#).
- [35] A. Abouelkomsan, A. P. Reddy, L. Fu, and E. J. Bergholtz, “Band mixing in the quantum anomalous hall regime of twisted semiconductor bilayers,” (2023), [arXiv:2309.16548 \[cond-mat.mes-hall\]](#).
- [36] C. Xu, J. Li, Y. Xu, Z. Bi, and Y. Zhang, “Maximally localized wannier orbitals, interaction models and fractional quantum anomalous hall effect in twisted bilayer mote_2 ,” (2024), [arXiv:2308.09697 \[cond-mat.str-el\]](#).
- [37] J. Dong, T. Wang, T. Wang, T. Soejima, M. P. Zaletel, A. Vishwanath, and D. E. Parker, “Anomalous Hall Crystals in Rhombohedral Multilayer Graphene I: Interaction-Driven Chern Bands and Fractional Quantum Hall States at Zero Magnetic Field,” (2023), [arXiv:2311.05568 \[cond-mat\]](#).
- [38] J. Wang, J. Cano, A. J. Millis, Z. Liu, and B. Yang, “Exact landau level description of geometry and interaction in a flatband,” *Phys. Rev. Lett.* **127**, 246403 (2021).
- [39] N. Morales-Durán, N. Wei, and A. H. MacDonald, “Magic angles and fractional chern insulators in twisted homobilayer tmds,” [arXiv preprint arXiv:2308.03143](#) (2023).
- [40] M. O. Goerbig, “From fractional chern insulators to a fractional quantum spin hall effect,” *The European Physical Journal B* **85**, 15 (2012).
- [41] R. Roy, “Band geometry of fractional topological insulators,” *Phys. Rev. B* **90**, 165139 (2014).
- [42] T. S. Jackson, G. Möller, and R. Roy, “Geometric stability of topological lattice phases,” *Nature communications* **6**, 1–11 (2015).
- [43] M. Claassen, C. H. Lee, R. Thomale, X.-L. Qi, and T. P. Devereaux, “Position-momentum duality and fractional quantum hall effect in chern insulators,” *Phys. Rev. Lett.* **114**, 236802 (2015).
- [44] T. Ozawa and B. Mera, “Relations between topology and the quantum metric for chern insulators,” *Phys. Rev. B* **104**, 045103 (2021).
- [45] B. Mera and T. Ozawa, “Kähler geometry and chern insulators: Relations between topology and the quantum metric,” *Phys. Rev. B* **104**, 045104 (2021).
- [46] D. Varjas, A. Abouelkomsan, K. Yang, and E. J. Bergholtz, “Topological lattice models with constant Berry curvature,” *SciPost Phys.* **12**, 118 (2022).
- [47] B. Mera and T. Ozawa, “Engineering geometrically flat chern bands with fubini-study kähler structure,” *Phys. Rev. B* **104**, 115160 (2021).
- [48] J. Wang and Z. Liu, “Hierarchy of ideal flatbands in chiral twisted multilayer graphene models,” *Phys. Rev. Lett.* **128**, 176403 (2022).
- [49] P. J. Ledwith, A. Vishwanath, and E. Khalaf, “Family of ideal chern flatbands with arbitrary chern number in chiral twisted graphene multilayers,” *Phys. Rev. Lett.* **128**, 176404 (2022).
- [50] B. Mera, A. Zhang, and N. Goldman, “Relating the topology of Dirac Hamiltonians to quantum geometry: When the quantum metric dictates Chern numbers and winding numbers,” *SciPost Phys.* **12**, 018 (2022).
- [51] A. Abouelkomsan, K. Yang, and E. J. Bergholtz, “Quantum metric induced phases in moiré materials,” *Phys. Rev. Res.* **5**, L012015 (2023).
- [52] B. Estienne, N. Regnault, and V. Crépel, “Ideal chern bands as landau levels in curved space,” *Phys. Rev. Res.* **5**, L032048 (2023).
- [53] P. J. Ledwith, A. Vishwanath, and D. E. Parker, “Vortexability: A unifying criterion for ideal fractional chern insulators,” *Phys. Rev. B* **108**, 205144 (2023).
- [54] B. Hetényi and P. Lévy, “Fluctuations, uncertainty relations, and the geometry of quantum state manifolds,” *Phys. Rev. A* **108**, 032218 (2023).
- [55] J. P. Provost and G. Vallee, “Riemannian structure on manifolds of quantum states,” *Communications in Mathematical Physics* **76**, 289–301 (1980).
- [56] R. Cheng, “Quantum geometric tensor (fubini-study metric) in simple quantum system: A pedagogical introduction,” [arXiv preprint arXiv:1012.1337](#) (2010), 10.48550/ARXIV.1012.1337.
- [57] G. Tarnopolsky, A. J. Kruchkov, and A. Vishwanath, “Origin of magic angles in twisted bilayer graphene,” *Phys. Rev. Lett.* **122**, 106405 (2019).
- [58] J. Behrmann, Z. Liu, and E. J. Bergholtz, “Model fractional chern insulators,” *Phys. Rev. Lett.* **116**, 216802 (2016).
- [59] A. M. Läuchli, Z. Liu, E. J. Bergholtz, and R. Moessner, “Hierarchy of fractional chern insulators and competing compressible states,” *Phys. Rev. Lett.* **111**, 126802 (2013).
- [60] In this supplemental material, we provide the details of the interaction Hamiltonian, the evidence of particle-hole symmetry breaking at other fillings, the spectral flow with respect to magnetic flux insertion, the choice of samples, and the relation between the hole energy and the quantum geometry..
- [61] F. D. M. Haldane, “Fractional quantization of the hall effect: A hierarchy of incompressible quantum fluid states,” *Phys. Rev. Lett.* **51**, 605–608 (1983).
- [62] A. P. Reddy and L. Fu, “Toward a global phase diagram of the fractional quantum anomalous hall effect,” *Phys. Rev. B* **108**, 245159 (2023).
- [63] B. A. Bernevig and N. Regnault, “Emergent many-body translational symmetries of Abelian and non-Abelian fractionally filled topological insulators,” *Physical Review B* **85**, 075128 (2012).
- [64] H. Li and F. D. M. Haldane, “Entanglement Spectrum as a Generalization of Entanglement Entropy: Identification of Topological Order in Non-Abelian Fractional Quantum Hall Effect States,” *Physical Review Letters* **101**, 010504 (2008).

- [65] A. Sterdyniak, N. Regnault, and B. A. Bernevig, “Extracting Excitations from Model State Entanglement,” *Physical Review Letters* **106**, 100405 (2011).
- [66] M. S. Hossain, M. K. Ma, M. A. Mueed, D. Kamburov, L. N. Pfeiffer, K. W. West, K. W. Baldwin, R. Winkler, and M. Shayegan, “Geometric resonance of four-flux composite fermions,” *Phys. Rev. B* **100**, 041112 (2019).
- [67] J. Wang, “Dirac fermion hierarchy of composite fermi liquids,” *Phys. Rev. Lett.* **122**, 257203 (2019).
- [68] P. Wilhelm, T. C. Lang, and A. M. Läuchli, “Interplay of fractional chern insulator and charge density wave phases in twisted bilayer graphene,” *Phys. Rev. B* **103**, 125406 (2021).
- [69] B. A. Bernevig, Z.-D. Song, N. Regnault, and B. Lian, “Twisted bilayer graphene. iii. interacting hamiltonian and exact symmetries,” *Phys. Rev. B* **103**, 205413 (2021).
- [70] D. Parker, P. Ledwith, E. Khalaf, T. Soejima, J. Hauschild, Y. Xie, A. Pierce, M. P. Zaletel, A. Yacoby, and A. Vishwanath, “Field-tuned and zero-field fractional chern insulators in magic angle graphene,” *arXiv preprint arXiv:2112.13837* (2021).
- [71] See Supplemental material for details about the definition of the quantum metric, the projected interacting Hamiltonian and additional results regarding the hole dispersion.
- [72] C. Repellin, B. A. Bernevig, and N. Regnault, “ \mathbb{Z}_2 fractional topological insulators in two dimensions,” *Phys. Rev. B* **90**, 245401 (2014).

SUPPLEMENTAL MATERIALS TO ‘BROKEN SYMMETRY IN IDEAL CHERN BANDS’

In this supplemental material, we provide the details of the interaction Hamiltonian, the evidence of particle-hole symmetry breaking at other fillings, the spectral flow with respect to magnetic flux insertion, the choice of samples, and the relation between the hole energy and the quantum geometry.

THE INTERACTION HAMILTONIAN AND THE SINGLE-HOLE DISPERSION

The two-body interaction projected to a single band with specific valley and spin takes the form of

$$H^{\text{proj}} = \sum_{\mathbf{k}_1, \mathbf{k}_2, \mathbf{k}_3, \mathbf{k}_4} V_{\mathbf{k}_1 \mathbf{k}_2 \mathbf{k}_3 \mathbf{k}_4} c_{\mathbf{k}_1}^\dagger c_{\mathbf{k}_2}^\dagger c_{\mathbf{k}_3} c_{\mathbf{k}_4}, \quad (4)$$

with the interaction matrix element

$$V_{\mathbf{k}_1 \mathbf{k}_2 \mathbf{k}_3 \mathbf{k}_4} = \frac{1}{2} \sum_{\mathbf{q}} V(\mathbf{q}) \sum_{\tau, \tau'} \sum_{\{m, n\}=-d}^d \delta_{\mathbf{k}_1 + \mathbf{k}_2 + (m_1 + m_2)\mathbf{G}_1 + (n_1 + n_2)\mathbf{G}_2, \mathbf{k}_3 + \mathbf{k}_4 + (m_3 + m_4)\mathbf{G}_1 + (n_3 + n_4)\mathbf{G}_2} \cdot \\ \delta_{\mathbf{k}_1 - \mathbf{k}_4 + (m_1 - m_4)\mathbf{G}_1 + (n_1 - n_4)\mathbf{G}_2, \mathbf{q}} \mu_{m_1, n_1, \tau}^*(\mathbf{k}_1) \mu_{m_2, n_2, \tau'}^*(\mathbf{k}_2) \mu_{m_3, n_3, \tau'}(\mathbf{k}_3) \mu_{m_4, n_4, \tau}(\mathbf{k}_4). \quad (5)$$

Here, $V(\mathbf{q})$ indicates either the pseudopotential-like short-range interaction or the bare Coulomb interaction, \mathbf{G}_1 and \mathbf{G}_2 denote the two moiré reciprocal operators, respectively, and τ (τ') represents the orbital index. $\mu_{m,n}(\mathbf{k})$ is the eigenvector of the valence and topological flat band at $m\mathbf{G}_1 + n\mathbf{G}_2$ sector for momentum $\mathbf{k} \in \text{MBZ}$. In numerical simulations, we choose a cutoff $d = 8$, which is enough to make both the single-particle bandstructure and the many-body energy spectrum converge.

The breaking of particle-hole symmetry is originated from the inhomogeneous single-hole dispersion $E_h(\mathbf{k})$ (in other words, not a constant). Here, we derive the concrete form of $E_h(\mathbf{k})$. The original interaction Hamiltonian in momentum space reads,

By doing the particle-hole transformation $c_{\mathbf{k}}^\dagger \rightarrow c_{\mathbf{k}}$, we have

$$H^{\text{proj}} \rightarrow \sum_{\mathbf{k}_1, \mathbf{k}_2, \mathbf{k}_3, \mathbf{k}_4} V_{\mathbf{k}_1 \mathbf{k}_2 \mathbf{k}_3 \mathbf{k}_4} c_{\mathbf{k}_1}^\dagger c_{\mathbf{k}_2}^\dagger c_{\mathbf{k}_3} c_{\mathbf{k}_4} + \sum_{\mathbf{k}} E_h(\mathbf{k}) c_{\mathbf{k}}^\dagger c_{\mathbf{k}}, \quad (6)$$

with $E_h(\mathbf{k}) = \sum_{\mathbf{k}'} (V_{\mathbf{k}'\mathbf{k}\mathbf{k}'\mathbf{k}} + V_{\mathbf{k}\mathbf{k}'\mathbf{k}\mathbf{k}'} - V_{\mathbf{k}\mathbf{k}'\mathbf{k}'\mathbf{k}} - V_{\mathbf{k}'\mathbf{k}\mathbf{k}\mathbf{k}'}).$

SPECTRAL FLOW FOR $\nu = 1/3$ AND $3/7$

Here, we examine the topological nature of the system at band filling $\nu = 1/3$ and $3/7$ by introducing an external magnetic flux. As shown in Fig. 5, for both fillings, the quasi-degenerate FCI ground states remain isolated from the ground states, and evolve into each other with the magnetic flux, which indicates their corresponding fractional transmission.

RESULTS OF OTHER FILLINGS

In this section, we provide a detailed study for other fillings. Like the FQHE in the LLL, varying the partial filling of the flat band in cTBG ν , from $1/3$ to $1/2$ (here, we choose $\nu = 2/5, 3/7$, and $4/9$), indeed leads to a energy gap closing between FCI ground states and excitation states, shown in Fig. 6(a1-c1).

At $\nu = 2/5$, five quasi-degenerate ground states appear at momentum sectors satisfying the Haldane statistics and are separated from excitation states with a clear energy gap.

For $\nu = 3/7$, although the energy gap is less conspicuous, seven quasi-degenerate ground states persist at the right momentum sectors, maintaining isolation from other states. This is further validated by introducing a magnetic flux, where the seven ground states never mix with other higher energy states, making the energy gap visible. Alternatively, employing a tilted sample configuration reveals the clear separation of the seven ground states from excitation states (see Fig. 7(a)).

Approaching $\nu = 4/9$, near the phase transition, both clear FCI ground states and energy gap are absent, as evident from both the rectangular sample, shown in Fig. 6(c1) and the tilted sample shown in Fig. 7(c)

We then shift the focus to band filling within $(1/2, 2/3)$, specifically, $\nu = 3/5, 4/7$, and $5/9$, the complimentary partners. Surprisingly, the energy spectrum of each of these fillings, both from the rectangular sample and the tilted shows an absence of

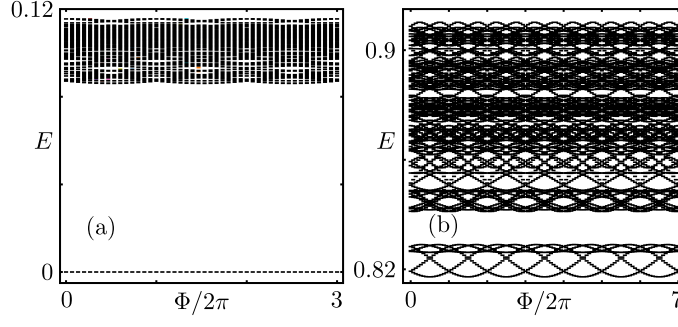


FIG. 5. The low-lying energy spectrum as a function of magnetic flux Φ at band filling $\nu = 1/3$ (a) and $3/7$ (b) with a system size 4×6 and 4×7 clusters, respectively. Here, we use a pseudopotential-like short-range interaction.

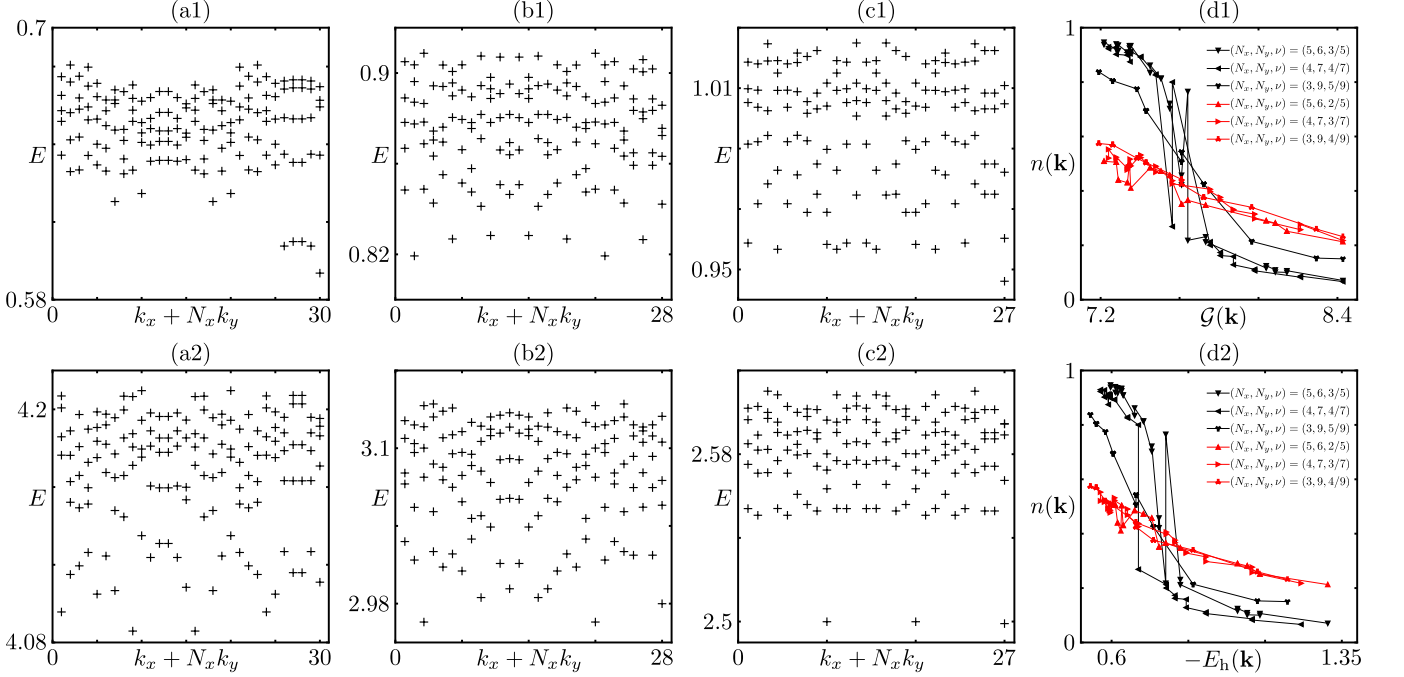


FIG. 6. (a1-c1) are the low-lying energy spectrum for band filling $\nu = 2/5, 3/7$, and $4/9$, at system size $5 \times 6, 4 \times 7$, and 3×9 clusters, respectively. (a2-c2) are the energy spectrum for their complementary band fillings $\nu = 3/5, 3/7$, and $5/9$, respectively. (d1) and (d2) are the occupation number of ground states at different fillings as a function of quantum geometry and the single-hole dispersion, respectively. Here, we use a pseudopotential-like short-range interaction and only selective five lowest energies in ED simulations.

FCI ground states or an associated energy gap. This is again opposite to the conventional understanding that the flat band in cTBG has an identical physics with the LLL, where the presence of a FCI phase is expected.

We further apply an analysis of the occupation number, like what we have discussed in the main text, there is an emergent Fermi liquid formed for $\nu \in (1/2, 2/3)$, while for $\nu \in (1/3, 1/2)$, the system shows a FCI behavior, even for $\nu = 4/9$, which is quite close the phase transition at $\nu = 1/2$. This thus aligns with our main conclusion.

DETAILS ON THE NUMERICAL SIMULATIONS

In this section, we provide the geometry we use for the rectangular and tilted sample. Note that we run all ED simulations in momentum space. Here, the rectangular sample means we use the moiré reciprocal vectors \mathbf{G}_1 and \mathbf{G}_2 . For the tilted sample, the spanning vector is a linear combination of these two moiré reciprocal vectors [72].

All calculations on rectangular samples (Fig. 1, Fig. 2 in the main text, and Fig. 6 in this supplemental materials), are with system size (N_x, N_y) and spanning vectors $\mathbf{T}_1 = (N_x, 0)$ and $\mathbf{T}_2 = (0, N_y)$.

In the calculation of the charge density wave (Fig. 3 in this supplemental materials), we use two system sizes. For the case

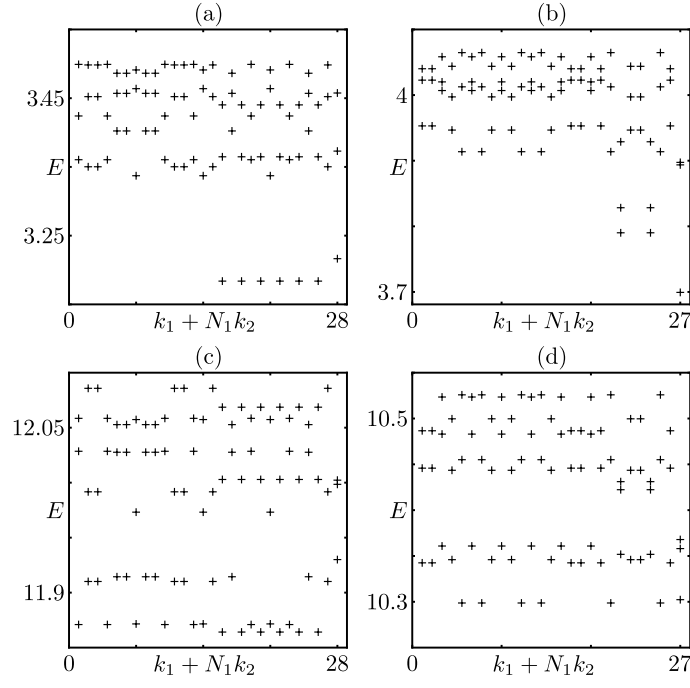


FIG. 7. (a-b) the low-lying energy spectrum of the tilted sample for banding filling $\nu = 3/7$ and $4/9$, at system size 4×7 and 3×9 clusters, respectively. (c-d) are the energy spectrum of their particle-hole partner $\nu = 4/7$ and $5/9$, respectively. Here, we use a pseudopotential-like short-range interaction and only selective three lowest energies in ED simulations.

of 32 sites, we use the spanning vectors $\mathbf{T}_1 = (2, -4)$ and $\mathbf{T}_2 = (6, 4)$. For the case of 36 sites, we use the spanning vectors $\mathbf{T}_1 = (6, 0)$ and $\mathbf{T}_2 = (0, 6)$.

In the calculation of the energy spectrum of tilted samples (Fig. 7 in this supplemental materials), for band filling $\nu = 3/7$ and $4/7$, we use a system size 28 clusters, and the spanning vectors $\mathbf{T}_1 = (4, -2)$ and $\mathbf{T}_2 = (2, 6)$. At band filling $\nu = 4/9$ and $5/9$, we use a system size 27 clusters, and the spanning vectors $\mathbf{T}_1 = (6, 3)$ and $\mathbf{T}_2 = (3, 6)$.

We note that, the energy scale difference between the rectangular sample and the tilted sample, shown in Fig. 6 and Fig. 7, is up to a constant in numerical simulations.

HOLE DISPERSION AND BAND GEOMETRY

The Bloch wavefunction of an ideal Chern band takes the form $\psi_{\mathbf{k}}(\mathbf{r}) = N_{\mathbf{k}} B(\mathbf{r}) \phi_{\mathbf{k}}^{\text{LLL}}(\mathbf{r})$ where $N_{\mathbf{k}}$ is a k -dependent normalization, and $B(\mathbf{r})$ is a k -independent quasi-periodic function with $\phi_{\mathbf{k}}^{\text{LLL}}(\mathbf{r})$ the LLL wavefunction. Therefore the matrix elements $V_{\mathbf{k}_1 \mathbf{k}_2 \mathbf{k}_3 \mathbf{k}_4}$ are related to the LLL form factors [38] as

$$V_{\mathbf{k}_1 \mathbf{k}_2 \mathbf{k}_3 \mathbf{k}_4} = \left(\prod_{i=1}^4 N_{\mathbf{k}_i} \right) F_{\mathbf{k}_1 \mathbf{k}_2 \mathbf{k}_3 \mathbf{k}_4} \quad (7)$$

where $F_{\mathbf{k}_1 \mathbf{k}_2 \mathbf{k}_3 \mathbf{k}_4}$ is a function of the LLL form factors and the interactions. The normalization factor $N_{\mathbf{k}}$ is the major difference from a LL and controls the band geometry fluctuations. The Berry curvature $\Omega_{\mathbf{k}}$ and the FS metric is given by $|\Omega_{\mathbf{k}}| = |-1 + \Delta_{\mathbf{k}} \log N_{\mathbf{k}}| = \text{tr } g_{\mathbf{k}}$, where $\Delta_{\mathbf{k}}$ is the Laplacian operator. The hole energy is related to the normalization factor as

$$E_h(\mathbf{k}) = N_{\mathbf{k}}^2 \sum_{\mathbf{k}'} N_{\mathbf{k}'}^2 (F_{\mathbf{k} \mathbf{k}' \mathbf{k} \mathbf{k}'} + F_{\mathbf{k}' \mathbf{k} \mathbf{k}' \mathbf{k}} - F_{\mathbf{k} \mathbf{k}' \mathbf{k}' \mathbf{k}} - F_{\mathbf{k}' \mathbf{k} \mathbf{k} \mathbf{k}'}) \quad (8)$$

So in ideal bands, there is an even closer connection between hole dispersion and the non-uniformity of the quantum geometry, directly from the normalization $N_{\mathbf{k}}$ which controls the fluctuations of Berry curvature and FS metric.